Available online at www.sciencedirect.com
ScienceDirect
Journal of Power Sources 167 (2007) 100–110
JOURNAL OF POWER SOURCES
www.elsevier.com/locate/jpowsour

Electrochemical AC impedance model of a solid oxide fuel cell and its application to diagnosis of multiple degradation modes

J.I. Gazzarri *, O. Kesler

Department of Mechanical Engineering, University of British Columbia, 2054-6250 Applied Science Lane, Vancouver, BC V6T 1Z4, Canada

Received 19 December 2006; received in revised form 7 February 2007; accepted 8 February 2007
Available online 17 February 2007

Abstract

A finite element model of the impact of diverse degradation mechanisms on the impedance spectrum of a solid oxide fuel cell is presented as a tool for degradation mode identification. Among the degradation mechanisms that cause electrode active area loss, the attention is focused on electrode delamination and uniformly distributed surface area loss, which were found to cause distinct and specific changes in the impedance spectrum. Degradation mechanisms resulting in uniformly distributed reactive surface area loss include sintering, sulphur poisoning, and possibly incipient coke formation at the anode, and chromium deposition at the cathode. Parametric studies reveal the extent and limits of applicability of the model and detectability of the different degradation modes, as well as the influence of different cell geometries on the change in impedance behaviour resulting from the loss of active area. It is expected that this technique could form the basis of a useful diagnostic tool for both solid oxide fuel cell developers and users.
© 2007 Elsevier B.V. All rights reserved.

Keywords: Solid oxide fuel cell; Delamination; Degradation; Diagnostics; Sulphur poisoning; Chromium deposition

1. Introduction

Although SOFCs are an attractive alternative to fossil fuel combustion for power generation because of their high efficiency, their viability is still subject to the solution of problems associated with their reliability, durability, and cost. Cell degradation is an important phenomenon related to the first two of these categories. Many types of degradation mechanisms have been identified in SOFCs. They range from thermo-mechanical issues such as electrode delamination and electrolyte cracking, to thermo-chemical phenomena such as electrode poisoning and microstructure coarsening. The nature of these mechanisms is very diverse, and so are their potential corrective actions. Some of these degradation mechanisms are reversible, such as early stage carbon deposition [1] or sulphur poisoning [2], whereas others are irreversible, for example electrode delamination [3] and electrolyte cracking. Despite their difference in nature, the effect of these degradation modes on cell performance in long-term degradation testing is common to all of them: a loss in available potential at constant current load. In other words, it is not possible to identify a specific degradation mechanism or combination of mechanisms by observing only changes to the DC potential of the cell at constant current. Thus, there is a need to develop a diagnostic technique that allows the identification of a specific degradation mechanism of SOFCs in a minimally invasive way. Such a technique would be a useful tool for diagnosis of both a cell in service or under research, where identifying the nature of a degradation mechanism could save the disassembly time required for a direct observation. In the case of reversible degradation, the method would indicate the possibility to correct the failure while the fuel cell is in operation. In the case of irreversible degradation, the method would aid in identifying the specific cause of failure of a component that needs replacement, so that operating conditions or cell or stack materials or designs could potentially be adjusted in subsequent tests to minimize further degradation.

Impedance spectroscopy is a well-known technique used to study electrochemical characteristics of systems such as batteries, capacitors, and fuel cells, and which is widely used in disciplines such as corrosion and materials science. It consists of measuring the impedance of a system at different frequencies by superimposing a small voltage or current perturbation onto

* Corresponding author. Tel.: +1 604 822 4745; fax: +1 604 822 2403.
E-mail address: javier@mech.ubc.ca (J.I. Gazzarri).

0378-7753/$ – see front matter © 2007 Elsevier B.V. All rights reserved.
doi:10.1016/j.jpowsour.2007.02.010

the voltage or current operating point. The underlying idea is that individual processes will appear in the impedance spectrum at different frequencies, according to their inherent rate. For example, a charge transfer process is likely to appear at higher frequencies than a slower diffusional process. This technique is convenient because it is minimally invasive, and it can be used on systems in operation. Its resolution in frequency allows the separate study of simultaneous cell processes, potentially enabling their individual optimization. The method described in this work relies on impedance spectroscopy as a tool to characterize the SOFC and its degradation modes.

Among the various mechanical degradation modes that cause loss of active electrode area, electrode delamination has been commonly reported as a consequence of thermal or redox cycling that degrades the interface between adjacent layers [3]. The interruption of the ionic conduction path renders part of the electrode under-utilized, resulting in the cell losing almost the entire electrode area projected from the delamination in the main direction of the current [4]. Other degradation modes that cause a loss of active area include cathode chromium poisoning [5] and anode sulphur poisoning [2] and anode nickel sintering [6], in this case by blocking reaction sites or coarsening the electrode microstructure, respectively. These degradation modes are distributed through the electrode volumes, uniformly in the case of anode sintering, or more highly localized at triple phase boundaries, in the case of cathode chromium poisoning.

This work presents impedance modeling results that allow a comparison of the impact of delamination with that of other degradation mechanisms that involve a loss in electroactive surface area. Furthermore, the results for delamination and for these other mechanisms are compared among different geometrical cell configurations, such as anode, electrolyte, and interconnect-supported cells, and the effects of different layer thicknesses on the limits of resolution and detectability are presented.

2. Numerical model

An operational SOFC is modeled using finite elements. The geometry considered in the model is restricted to the anode–electrolyte–cathode system. Ongoing work expands the model to include the interconnect plates. Fig. 1a–c show the modeled geometries, which correspond to circular button cells, with 16mm diameter electrodes, in electrolyte (ESC), anode (ASC), and interconnect (ISC)-supported cell configurations. The circular geometry allows the 2D axi-symmetric simplification. The leftmost vertical centerline indicates the axi-symmetry axis. These layer thickness geometries correspond to those of typical planar SOFCs with the respective supporting layers, and the in-plane geometry corresponds to that of a standard laboratory scale button cell that is commonly used to study each type of fuel cell. Simulated materials are 8 mol% yttria-stabilized zirconia (8YSZ) for the electrolyte, a 50 vol% lanthanum strontium manganite (LSM)/50 vol% YSZ composite for the cathode, and a 40 vol% Ni/60 vol% YSZ composite for the anode, with both electrodes having 40% porosity. Electrochemical data were taken from the literature and from in-house experiments. These values are shown in Table 1. As a first approximation, the model

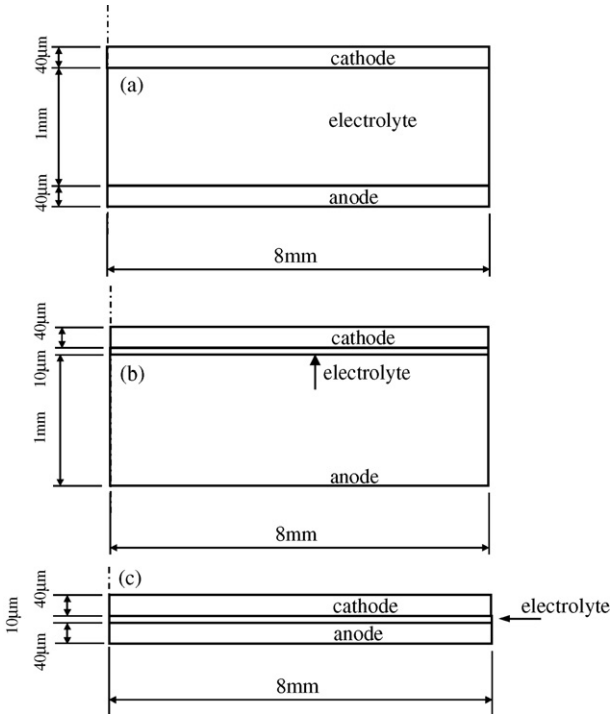

Fig. 1. Modeled axysimmetric geometry corresponding to a circular button cell whose electrode is 16 mm in diameter. (a) Electrolyte-supported configuration, (b) anode-supported configuration and (c) interconnect-supported configuration.

neglects any reactant concentration gradients, corresponding to very low fuel utilization and low current density, as well as any concentration polarization. The simulation is performed at OCV conditions. The system is also approximated as isothermal, a reasonable approximation for a small size cell.

This model consists of the solution of the charge transfer equations over the electrode and electrolyte volumes. The approach is based on modeling averaged porous composite properties as described in Newman and Tobias [7]. The solved unknowns are the electronic (in the electrodes) and ionic (electrodes and electrolyte) potentials, for both the AC and DC cases. The charge balance equation is, in general,

$$\nabla \cdot i = Si_{\mathrm{F}}(\eta) + SC_{\mathrm{dl}} \frac{\partial \eta}{\partial t}, \tag{1}$$

where i is the ionic or electronic current density vector (A m^{-2}), S the electrochemically active surface area of the medium per unit volume (m^{-1}), i_{F} the Faradaic current density (A m^{-2}), η the local overpotential (V), C_{dl} the double layer capacitance associated with the interface between the ionic and electronic conducting phases (F m^{-2}), and t is the time (s). The overpotential is defined as the difference between the potentials of the electronic (Φ_{ELE}) and ionic (Φ_{ION}) phases with respect to an equilibrium potential (Φ_{REF}):

$$\eta = \Phi_{\mathrm{ELE}} - \Phi_{\mathrm{ION}} - \Phi_{\mathrm{REF}} \tag{2}$$

Eq. (1) is the result of balancing the charge flux over a differential volume element. The difference between input and output of charge to the element is the Faradaic production or consumption of charge, plus the time-dependent charging of the

Table 1
Input parameters used in the model for calculation of the impedance behaviour of the intact cell

Property	Symbol	Value	Ref.
Operating point (V)	V	1	
Open circuit potential (V)	OCV	1	[9]
Volumetric anode exchange current density ($A\,m^{-3}$)	$S_{ANO}i_{0,ANO}$	2.2×10^7	[10]
Volumetric cathode exchange current density ($A\,m^{-3}$)	$S_{CAT}i_{0,CAT}$	2.2×10^7	[11–13]
Double layer capacitance, anode ($F\,m^{-2}$)	$C_{dl,ANO}$	0.4	[9]
Double layer capacitance, cathode ($F\,m^{-2}$)	$C_{dl,CAT}$	90	[11–13]
Electrolyte ionic conductivity ($S\,m^{-1}$)	$k_{ION,ELY}$	4.1	[9]
Effective anode ionic conductivity ($S\,m^{-1}$)	$k_{ION,ANO}$	0.29	[14]
Effective cathode ionic conductivity ($S\,m^{-1}$)	$k_{ION,CAT}$	0.24	[14]
Effective anode electronic conductivity ($S\,m^{-1}$)	$k_{ELE,ANO}$	4.8×10^3	[14]
Effective cathode electronic conductivity ($S\,m^{-1}$)	$k_{ELE,CAT}$	1.6×10^3	[14]
Temperature (°C)	T	850	
Peak to peak perturbation voltage (mV)	$\Delta\Phi_0^{AC}$	20	
Charge transfer coefficients, anode	$\alpha_{ANO,ANO}$; $\alpha_{ANO,CAT}$	2; 1	[15]
Charge transfer coefficients, cathode	$\alpha_{CAT,ANO}$; $\alpha_{CAT,CAT}$	1.5; 0.5	[16]

double layer. Ohm's law relates current density and the potential gradient:

$$i = -k\nabla\Phi, \tag{3}$$

where k is the effective (i.e. it considers porosity and tortuosity) conductivity for the species (ions or electrons) in the medium ($\Omega^{-1}\,m^{-1}$), and Φ is the electric (ionic or electronic) potential (V). Substituting the current density in Eq. (1) by the expression given by (3) yields

$$-\nabla\cdot(k\nabla\Phi) = Si_F(\eta) + SC_{dl}\frac{\partial\eta}{\partial t} \tag{4}$$

If the effective conductivity k is independent of the spatial coordinates, the divergence term becomes the Laplacian of the potential: $-k\nabla^2\Phi$. This assumption holds hereafter in this work. The Laplacian is expressed in axi-symmetric coordinates as:

$$k\nabla^2\Phi = k\left(\frac{1}{r}\frac{\partial}{\partial r}\left(r\frac{\partial\Phi}{\partial r}\right) + \frac{\partial^2\Phi}{\partial z^2}\right)$$

A further simplification of Eq. (4) is possible in the DC case, for which the time derivative vanishes, yielding:

$$-k\nabla^2\Phi = Si_F(\eta) \tag{5}$$

No double layer charging occurs in this case.

The source term relates the local (a.k.a. Faradaic) current denstity to the local overpotential. For example, the Faradaic ionic current generated in the DC cathodic reaction is given by

$$i_{F,ION,CAT}(\eta) = i_{0,CAT}\left[\exp\left(\frac{\alpha_{CAT,ANO}F}{RT}\eta_{CAT}\right) - \exp\left(-\frac{\alpha_{CAT,CAT}F}{RT}\eta_{CAT}\right)\right], \tag{6}$$

where $i_{0,CAT}$ is the cathodic exchange current density ($A\,m^{-2}$), α_{ij} the charge transfer coefficient for the reaction with the first subindex indicating the electrode and the second subindex indicating the anodic or cathodic direction, F the Faraday constant ($A\,s\,mol^{-1}$), R the universal gas constant ($J\,mol^{-1}\,K^{-1}$), and T is the absolute temperature (K). The reference potentials are those corresponding to open circuit against a reference electrode. Replacing the source term in Eq. (5) with the expression in Eq. (6) yields:

$$-k_{ION,CAT}\nabla^2\Phi_{ION} = S_{CAT}i_{0,CAT}\left[\exp\left(\frac{\alpha_{CAT,ANO}F}{RT}\eta_{CAT}\right) - \exp\left(-\frac{\alpha_{CAT,CAT}F}{RT}\eta_{CAT}\right)\right] \tag{7}$$

The charge conservation condition is obtained by setting the sum of the divergences of the ionic and electronic current densities equal to zero:

$$\nabla\cdot i_{ION} + \nabla\cdot i_{ELE} = 0 \tag{8}$$

Physically, this equation means that the total flux of current at the electrodes equals the sum of the electronic and ionic current fluxes. Mathematically, this relation indicates that the source term of the electronic current equivalent to Eq. (7) is numerically identical to that of Eq. (7), but with opposite sign. Similar equations are applicable to the anode side, using the appropriate anodic kinetic terms.

The only DC equation for the electrolyte corresponds to the ionic current balance, and the absence of electrochemical reactions in this domain implies that the Faradaic source term is equal to zero:

$$\nabla^2\Phi_{ION} = 0 \tag{9}$$

The resulting DC equations are solved for the electrical potentials with a finite element solver (Comsol Multiphysics, Comsol AB), using boundary conditions of the Dirichlet type for the electronic potentials at the current collectors:

$$\begin{aligned}\Phi_{ELE}|_{\text{cathode current collector}} &= V_{CELL}\\ \Phi_{ELE}|_{\text{anode current collector}} &= 0\,V\end{aligned} \tag{10}$$

Here V_{CELL} is the operating voltage of the cell. The electronic potential at all other boundaries, and all ionic potentials, have

Neumann (insulation) boundary conditions:

$$\frac{\partial \Phi}{\partial n} = 0 \tag{11}$$

The AC response of the system results from assuming linearity between input and output. This statement implies that the response to a sinusoidal potential perturbation is also sinusoidal and does not contain harmonics of different frequencies other than the perturbation frequency.

As an example, we consider the application of the charge balance in Eq. (4) to the ionic current in the cathode:

$$\begin{aligned} -k_{\mathrm{ION,CAT}}\nabla^2\Phi_{\mathrm{ION}} &= S_{\mathrm{CAT}}C_{\mathrm{dl,CAT}}\frac{\partial \eta_{\mathrm{CAT}}}{\partial t} \\ &+ S_{\mathrm{CAT}}i_{0,\mathrm{CAT}}\left[\exp\left(\frac{\alpha_{\mathrm{CAT,ANO}}F}{RT}\eta_{\mathrm{CAT}}\right)\right. \\ &\left. - \exp\left(-\frac{\alpha_{\mathrm{CAT,CAT}}F}{RT}\eta_{\mathrm{CAT}}\right)\right] \end{aligned} \tag{12}$$

Decomposing the total potential into its AC and DC parts:

$$\begin{aligned} \Phi_{\mathrm{ELE}} &= \Phi_{\mathrm{ELE}}^{\mathrm{DC}} + \Phi_{\mathrm{ELE}}^{\mathrm{AC}}\,\mathrm{e}^{\mathrm{j}\omega t} \\ \Phi_{\mathrm{ION}} &= \Phi_{\mathrm{ION}}^{\mathrm{DC}} + \Phi_{\mathrm{ION}}^{\mathrm{AC}}\,\mathrm{e}^{\mathrm{j}\omega t} \end{aligned} \tag{13}$$

and linearizing the resulting expression on account of the small size of the AC component, yields the following time-independent expression:

$$\begin{aligned} -k_{\mathrm{ION,CAT}}\nabla^2\Phi_{\mathrm{ION}}^{\mathrm{AC}} &= S_{\mathrm{CAT}}C_{\mathrm{dl,CAT}}\,\mathrm{j}\omega(\Phi_{\mathrm{ELE}}^{\mathrm{AC}} - \Phi_{\mathrm{ION}}^{\mathrm{AC}}) \\ &+ S_{\mathrm{CAT}}i_{0,\mathrm{CAT}}\frac{\alpha_{\mathrm{CAT,ANO}}F}{RT}(\Phi_{\mathrm{ELE}}^{\mathrm{AC}} - \Phi_{\mathrm{ION}}^{\mathrm{AC}}) \\ &\times \exp\left(\frac{\alpha_{\mathrm{CAT,ANO}}F}{RT}\eta_{\mathrm{CAT}}^{\mathrm{DC}}\right) \\ &+ S_{\mathrm{CAT}}i_{0,\mathrm{CAT}}\frac{\alpha_{\mathrm{CAT,CAT}}F}{RT}(\Phi_{\mathrm{ELE}}^{\mathrm{AC}} - \Phi_{\mathrm{ION}}^{\mathrm{AC}}) \\ &\times \exp\left(-\frac{\alpha_{\mathrm{CAT,CAT}}F}{RT}\eta_{\mathrm{CAT}}^{\mathrm{DC}}\right) \end{aligned} \tag{14}$$

Expressions analagous to Eq. (14) apply to each domain. These equations are simultaneously solved for a desired range of frequencies, usually between 1 MHz and 0.1 Hz, with the following boundary conditions:

$$\begin{aligned} \Phi_{\mathrm{ELE}}^{\mathrm{AC}}|_{\text{cathode current collector}} &= -\Delta\Phi_0^{\mathrm{AC}} \\ \Phi_{\mathrm{ELE}}^{\mathrm{AC}}|_{\text{anode current collector}} &= +\Delta\Phi_0^{\mathrm{AC}} \end{aligned}, \tag{15}$$

where $\Delta\Phi_0^{\mathrm{AC}}$ is the perturbation amplitude. Again, Neumann (insulation) boundary conditions apply everywhere else for the electronic potential, and everywhere for the ionic potentials.

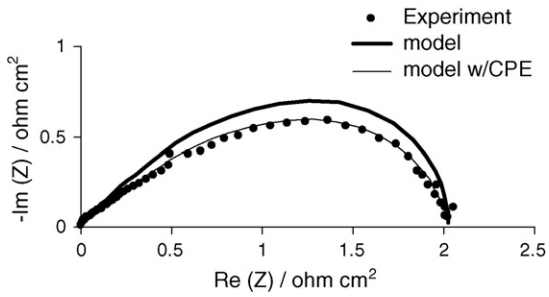

Fig. 2. Model result for a symmetric cathode button cell (thick solid line), compared to experimental data (dots). The model can reproduce the arc flattening using constant phase elements as the capacitative component in equation (14) (thin solid line). Conditions: 850 °C, air.

Using Eq. (3) it is possible to find all current densities, based on the calculated potentials.

$$\begin{aligned} i_{\mathrm{ION}}^{\mathrm{DC}} &= -k_{\mathrm{ION}}\nabla\Phi_{\mathrm{ION}}^{\mathrm{DC}} \\ i_{\mathrm{ELE}}^{\mathrm{DC}} &= -k_{\mathrm{ELE}}\nabla\Phi_{\mathrm{ELE}}^{\mathrm{DC}} \\ i_{\mathrm{ION}}^{\mathrm{AC}} &= -k_{\mathrm{ION}}\nabla\Phi_{\mathrm{ION}}^{\mathrm{AC}} \\ i_{\mathrm{ELE}}^{\mathrm{AC}} &= -k_{\mathrm{ELE}}\nabla\Phi_{\mathrm{ELE}}^{\mathrm{AC}} \end{aligned} \tag{16}$$

The impedance is the ratio between the applied voltage perturbation magnitude and the AC current density computed at either of the current collectors.

$$Z(\omega) = \frac{2\Delta\Phi_0^{\mathrm{AC}}}{i_{\mathrm{ELE}}^{\mathrm{AC}}(\omega)|_{\text{current collector}}} \tag{17}$$

Fig. 2 shows the result of this impedance model applied to an electrolyte-supported, symmetric cathode button cell (cathode–electrolyte–cathode), and its comparison to an experiment performed at 850 °C at OCV in air. The experimental cell consisted of a 1 mm thick 8YSZ (Inframat Advanced Materials, CT, USA) circular pellet, with screen printed composite cathodes (50 vol% LSM–50 vol% YSZ) on both sides. The impedance spectrum was obtained using a Solartron 1260 frequency response analyzer (London Scientific, ON, Canada), with no DC bias. Equivalent results obtained using different air flow rates confirmed the assumption of negligible diffusional effects for this experimental case. The electroactive surface area S and the cathode double layer capacitance are the only fitting parameters used to match the polarization resistance and the peak frequency, respectively. The high frequency intercept was subtracted from both spectra to allow a better comparison of the arc shapes. The model is able to adequately reproduce the experimental data, supporting the validity of the modeling assumptions for the comparison experimental case of a button cell with low fuel utilization and current density. The experimental arc shows a flatter shape, a phenomenon that has been attributed to the fractal nature of the interface or to a non-uniform distribution of microstructural properties [8]. The model could reproduce this flattening (thin line in Fig. 2) by adding a third adjustable parameter, namely an exponent γ affecting the $\mathrm{j}\omega C_{\mathrm{dl}}$ term in Eq. (14). This modification, however, does not improve the predictive capability of the model with respect to changes in polarization or series resistance or peak frequency resulting

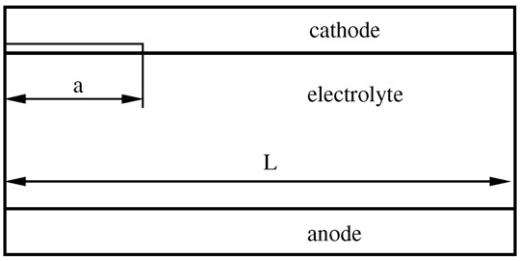

Fig. 3. Circular delamination of radius a at the centre of the circular cell, between the cathode and the electrolyte.

from cell degradation, since changes in the value of the exponent do not change those physical properties. This modification would imply representing the capacitive component of the electrochemical interface of the electrode with a constant phase element, as opposed to a capacitor. The impedance shown in Fig. 2 (thin line) was calculated using $\gamma = 0.88$. An exponent equal to unity corresponds to the case of an ordinary capacitor.

3. Results and discussion

3.1. Delamination

In the model, a delamination of the electrode is simulated by an array of elements with the dielectric properties of air inserted between the electrode and the electrolyte, as illustrated in Fig. 3, shown for the cathode delamination case. The indicated lengths correspond to radii of a circular cell. Therefore, the delamination constitutes a circular and concentric detachment of the electrode layer.

Fig. 4 shows a comparison of the spectra for electrolyte, anode, and interconnect-supported cell configurations (a: ESC, b: ASC, and c: ISC), for a delamination of 30% of the cathode

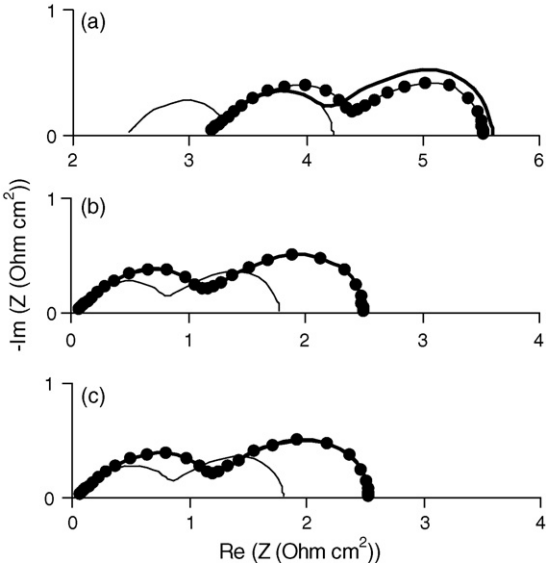

Fig. 4. Impedance spectra change caused by a cathode (bold lines) and anode (dotted lines) delamination of $a/L = 0.55$ (30% delaminated area) for different supporting configurations: (a) electrolyte-, (b) anode-, and (c) interconnect-supported cell.

Table 2
Changes in series and polarization resistances after 30% cathode or anode area delamination

	Cathode delamination			Anode delamination		
	ESC	ASC	ISC	ESC	ASC	ISC
R_S^0/R_S	0.780	0.712	0.710	0.776	0.708	0.709
R_P^0/R_P	0.725	0.713	0.713	0.755	0.711	0.715

R_S^0/R_S and R_P^0/R_P equal to 0.7 corresponds to the full-shadowing case, that is, total deactivation of the affected area by delamination. A larger number indicates that less than full shadowing has occurred.

or anode area, i.e. $a/L = 0.55$, with a equal to the radius of a concentric delamination, and L equal to the electrode radius. The thin line curves correspond to the spectra of the intact cell, the bold line curves indicate the spectra of the cathode-delaminated cell, and the dotted line represents the anode delamination case. Series and polarization resistances change as shown in Table 2, where we present this change in normalized resistance form. The normalized resistance is equal to the ratio of the original to post-degradation resistance, applied either to series or polarization resistance. Therefore, a value of unity corresponds to the intact state, and a value of zero represents total loss of performance.

The comparable increase in series and polarization resistance is attributed to a shadowing of the cell caused by the delamination, which essentially deactivates the regions above and below the delamination gap due to the high aspect ratio of the cell that makes in-plane ionic current conduction negligible compared to through-thickness conduction. In this example, a normalized resistance value of 0.7 (30% loss of performance) indicates full shadowing, whereas the shadowing is not total if this value is higher than 0.7. This effect is observed both for anode and for cathode delamination, and the extent of this shadowing is larger in thinner electrolytes. Fig. 5 shows the normalized DC ionic current density lines within the cell, ranging from magnitudes close to 0 (below the delamination) to 1 (within the unaffected region). It is apparent that very low in-plane conduction of oxide ions within the electrolyte renders the electrode volume above and below the delamination under-utilized.

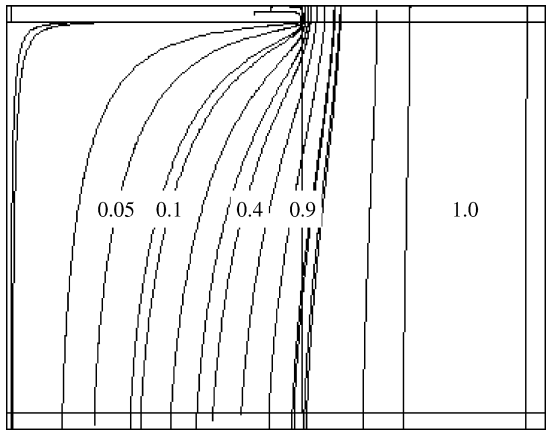

Fig. 5. Fractional DC ionic current density distribution illustrating the shadowing effect created by a cathode delamination of 30% of the total electrode area. A value of unity indicates the maximum current density for the modeled case. The current density is very low in the region below the delamination.

Table 3
Changes in series and polarization resistances after 30% cathode delamination, for different cell geometries, all for an anode-supported configuration

Electrolyte thickness (μm)	5	10	20
R_S^0/R_S	0.712	0.712	0.712
R_P^0/R_P	0.712	0.713	0.713
Anode thickness (μm)	500	700	1000
R_S^0/R_S	0.711	0.711	0.712
R_P^0/R_P	0.713	0.713	0.713
Cathode thickness (μm)	10	20	40
R_S^0/R_S	0.715	0.714	0.712
R_P^0/R_P	0.715	0.714	0.713

From top row: different electrolyte thicknesses (μm), different anode thicknesses (μm), and different cathode thicknesses (μm).

An illustrative way to visualize the change in series and in polarization resistance as a function of active area loss caused by delamination is shown in Fig. 6. Here, the normalized resistance change is shown as a function of the fraction of electrode area lost by delamination, for: (a) electrolyte-, (b) anode-, and (c) interconnect-supported configurations. The normalized ratio for the intact cell corresponds to unity, and for the completely delaminated cell corresponds to zero. In this way, it is possible to compare both resistances consistently, as a function of lost cell area. Fig. 6 indicates that delamination affects both polarization and series resistance in the same proportion, due to destruction of reaction sites and of conduction area, respectively. Due to the aforementioned very low in-plane ionic conduction, the shadowing is more complete in the thin-electrolyte cases, i.e. ASC and ISC. The A/A_0 line corresponds to the complete shadowing case, in which the area above and below the delamination has been completely deactivated.

From an experimental standpoint it is expected that the series resistance change caused by a small fraction of delaminated area would be difficult to detect in the case of cells with thin electrolytes (ASC and ISC cases), since the increase represents a small fraction of a small number. For example, the series resistance change in this case is 0.02 Ω cm^2 for both the ASC and ISC cases, a value that may be within the experimental scatter of an impedance measurement. The change in series resistance for the ESC case, on the other hand, is 0.7 Ω cm^2, a change that is much easier to detect within experimental tolerances.

Because of the variety of SOFC geometrical configurations in use, a study of the influence of different layer thicknesses on the detectability of delamination was performed. Figs. 7–9 show the aforementioned case of 30% area loss by cathode delamination on anode-supported cells for: three different electrolyte thicknesses (Fig. 7), three different anode thicknesses (Fig. 8), and three different cathode thicknesses (Fig. 9). Again, the intact case is given in thin lines for comparison. The results for changes in series and polarization resistances are shown in Table 3. The only case where a layer thickness may influence detectability within the range of thicknesses studied is in the case of a thin cathode (<40 μm), i.e., one for which the electrode volume is fully utilized, and for which a thicker cathode, by providing more reaction sites, would increase the fuel cell performance. In this case, the larger initial polarization resistance of the thin

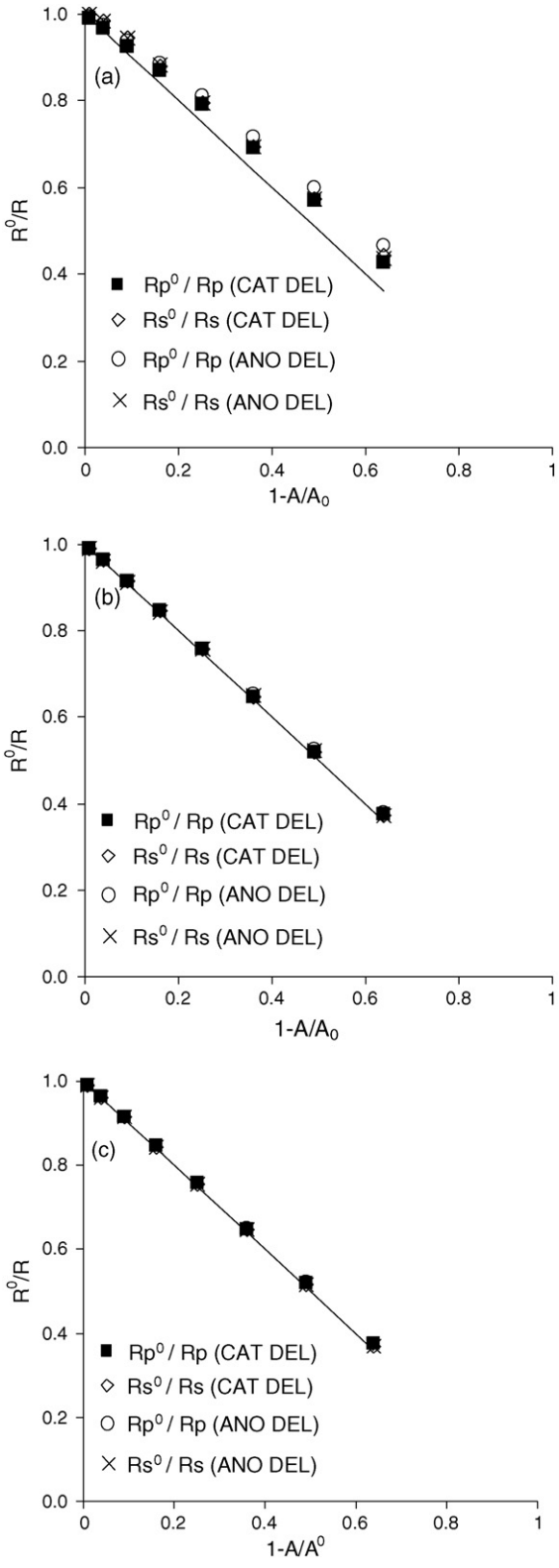

Fig. 6. Normalized polarization resistance and normalized series resistance as a function of the fraction of delaminated cathode area (solid square: R_P^0/R_P, empty diamond: R_S^0/R_S), and of the fraction of delaminated anode area (empty circle: R_P^0/R_P, cross: R_S^0/R_S). The line A/A_0 is plotted for comparison. Both polarization and series resistances scale with the extent of area loss, with no substantial difference between cathode or anode delamination. (a) ESC, (b) ASC and (c) ISC.

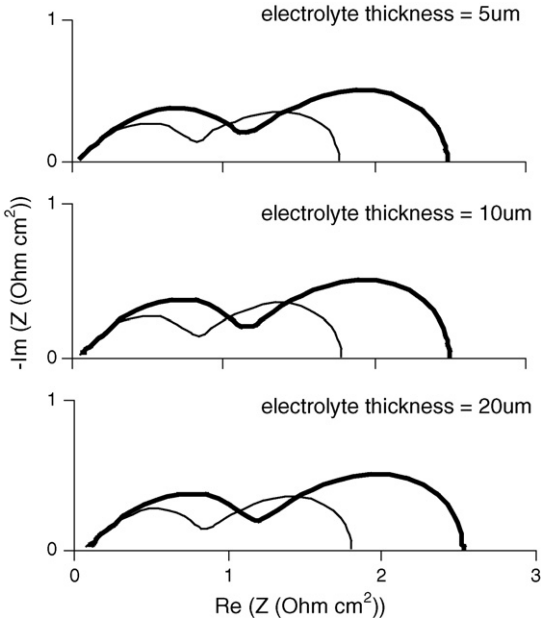

Fig. 7. Effect of electrolyte thickness on the impedance of an anode-supported cell with 30% delaminated cathode area. Thin lines: intact case; bold lines: delaminated case.

cathode makes it easier to identify a change in polarization resistance caused by a detachment of the cathode. In all of the cases with varying layer thicknesses, the same fundamental increase of polarization and series resistances in proportion to the delaminated area occurs, regardless of the cell geometry. This result suggests that even with increasing layer thicknesses within the range of typical ASC SOFC layer geometries, the large aspect ratio of the cell cannot be compensated, and so the shadowing of active sites occurs for thicker electrode and electrolyte layers as

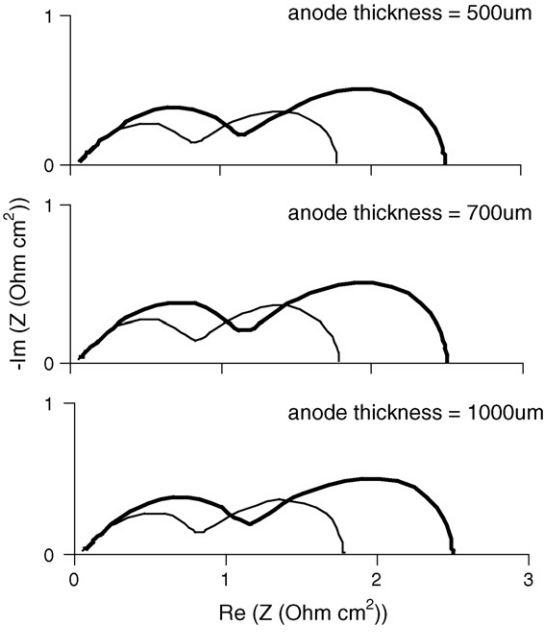

Fig. 8. Effect of anode thickness on the impedance of an anode-supported cell with 30% delaminated cathode area. Thin lines: intact case; bold lines: delaminated case.

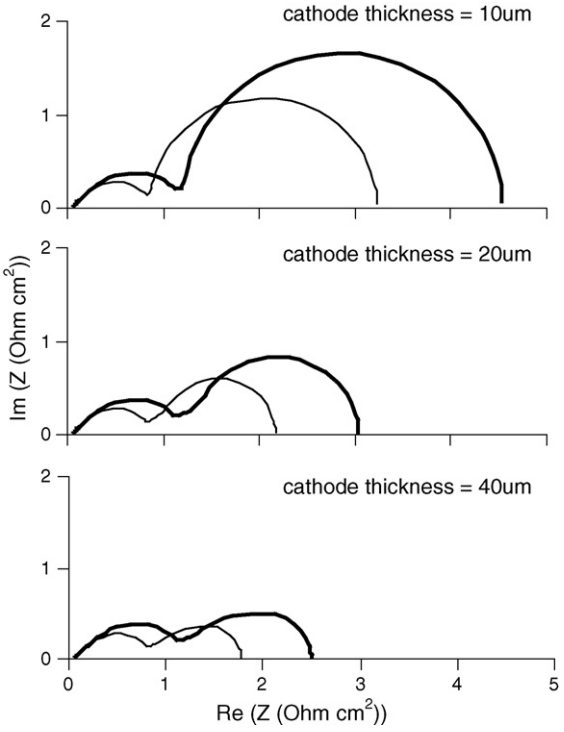

Fig. 9. Effect of cathode thickness on the impedance of an anode-supported cell with 30% delaminated cathode area. Thin lines: intact case; bold lines: delaminated case.

it does for thin layers. Performance loss is slightly more serious for thinner electrolyte configurations, but the difference in resistance change between the thinner and thicker electrolyte cases is likely too small to be detected experimentally in an ASC.

3.2. Loss of electro-active surface area

Electrode delamination degrades the SOFC performance by making the affected part of the cell area unusable. This phenomenon can be interpreted as a direct loss of electrochemically active surface area for reaction. Although other degradation mechanisms such as anode sintering, incipient coke formation, and chromium or sulphur poisoning also cause a loss in electrode electrochemically active surface area, the impedance behaviour changes observed as a result of these degradation mechanisms are qualitatively and quantitatively distinct from those corresponding to delamination, and proper interpretation of the impedance spectra could yield useful insight into the cell condition. These mechanisms affect the cell performance by uniformly decreasing the electroactive surface area available for reaction. In terms of the present model, they correspond to a decrease in the value of S in Eq. (1).

Fig. 10 shows the impedance spectra of an electrolyte-supported cell with four different scenarios of 30% active surface area loss, compared to the intact cell spectrum. In the first case we simulate a 30% reduction of S_{CAT}, the cathode active surface area, such as that which could result from chromium deposition covering 30% of the triple phase boundary reaction sites of the cathode. In the second case, we show a 30% reduction of S_{ANO}, the anode active surface area, such as that which could result

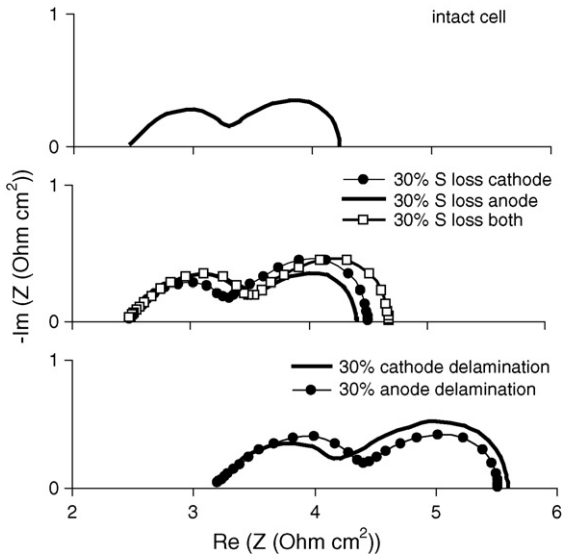

Fig. 10. Impedance spectrum differences among different degradation mechanisms that produce 30% loss of active surface area. From top to bottom: (1) intact cell, (2) 30% uniform surface area loss at the anode, cathode, and at both electrodes, (3) cathode and anode 30% area loss by delamination.

from anode sintering resulting in a 30% reduction in total anodic surface area, or from sulphur poisoning with a sulphur species covering 30% of the active reaction sites at the anode, while leaving other reaction sites essentially intact. In the third case, we show a 30% reduction of both anode and cathode active surface areas, corresponding physically to both mechanisms described above occurring simultaneously, in order to allow a more quantitative comparison with the behaviour of a delaminated cell, in which both electrodes become under-utilized due to a shadowing effect caused by the delamination. In the last case, we show the result of 30% of the cathode area and, separately, of 30% of the anode area having delaminated from the electrolyte.

While the arc diameters (R_P) of the degraded electrodes slightly increase in each of the three cases of uniformly distributed surface area, both arc diameters increase, and to a larger extent, in the case of delamination. Moreover, the high frequency intercept (R_S) only increases in the case of delamination, since only here does the conductive area change. This statement assumes that the influence of current constriction is negligible. The reason for the difference in the extent of polarization resistance change is less obvious. An electrode delamination implies a practically total loss of the reactive surface areas above and below the delamination. On the other hand, a reactive surface area decrease that is distributed uniformly throughout the electrode volume is expected to cause a less severe deterioration of performance, since it also produces a redistribution of electrochemical activity over any electrode area that was not previously fully utilized. This effect is more apparent for thick electrodes, where the performance loss is less abrupt than in cells with thin electrodes. These changes in the polarization and series resistances are summarized in Table 4.

Fig. 11 shows the same fractional changes in resistances as in Fig. 6, but as a function of the fractional uniform change in active electrode surface area, for each electrode individually, and

Table 4
Changes in series and polarization resistances after 30% electroactive surface area loss in the anode, cathode, and both electrodes for an ESC

	Anode	Cathode	Both
R_S^0/R_S	0.998	1.000	0.998
R_P^0/R_P	0.910	0.867	0.799

The series resistance remains essentially unaffected, while the polarization resistance suffers different changes according to the characteristics of the degraded electrode(s).

for both electrodes simultaneously. Similarly to the delamination case in Fig. 6, the abscissa variable is normalized such that a value of zero corresponds to the intact cell, while a value of one indicates total active surface area loss. In this case, there is essentially no change in the series resistance, while the polarization resistance changes, but to a lower extent compared to the cell delamination case. Keeping in mind that the closer the normalized resistance R^0/R gets to the S/S_0 line, the more severe the extent of degradation, it is apparent in Fig. 11 that cell performance will decrease to a slightly larger extent in the case of cathode uniform surface area loss than it will in the case of anode surface area loss. This statement is valid for an equivalent amount of surface area loss, and for electrodes of equal thickness.

The less severe degradation in cell performance due to uniform surface area loss compared to the equivalent amount of surface area loss caused by delamination is related to the uneven utilization of electrode thickness for electrochemical reaction. In the intact state, there is an uneven utilization of the electrode: the local Faradaic current production or consumption tapers down away from the interface with the electrolyte. This fact is reflected in the changing magnitude of the current density over the cathode thickness (Fig. 12). If the surface area decreases uniformly throughout the electrode volume, this local current profile changes so that the electrode volume is relatively

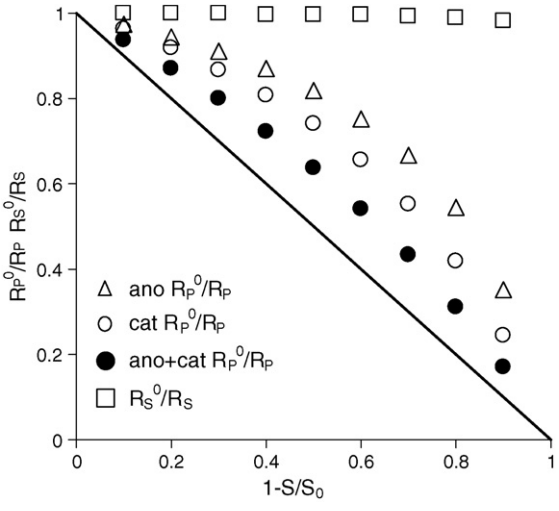

Fig. 11. Normalized polarization resistance and normalized series resistance as a function of the fraction of uniform surface area loss in the anode, cathode, and in both electrodes for an ESC with 40 μm thick electrodes. The line S/S_0 is plotted for comparison.

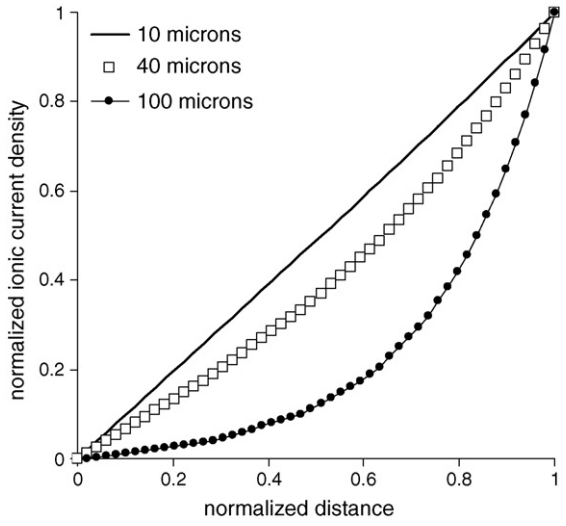

Fig. 12. Normalized ionic current density over the cathode thickness for three different cathode thicknesses, showing the different extents of volume utilization. The abscissa value is also normalized such that a value of abscissa equal to zero corresponds to the current collector, and a value equal to one corresponds to the interface with the electrolyte. The electrode is more uniformly utilized on thin electrodes than on thick electrodes, where most of the reaction takes place in the volume fraction of the electrode closest to the electrolyte.

more fully utilized further away from the electrolyte interface. In this case, the electrochemical reaction takes place more evenly throughout the electrode thickness, as shown in Fig. 13. This behaviour implies that the detrimental effect on performance of the mechanisms that degrade the electrode microstructure is less severe for thicker electrodes, under the assumption that all other processes, such as diffusion, remain unchanged by the loss in active surface area (a reasonable assumption for adsorption of a monolayer of sulphur-containing species on a portion of the anode reaction sites; less so for the case of surface area loss caused by anode sintering).

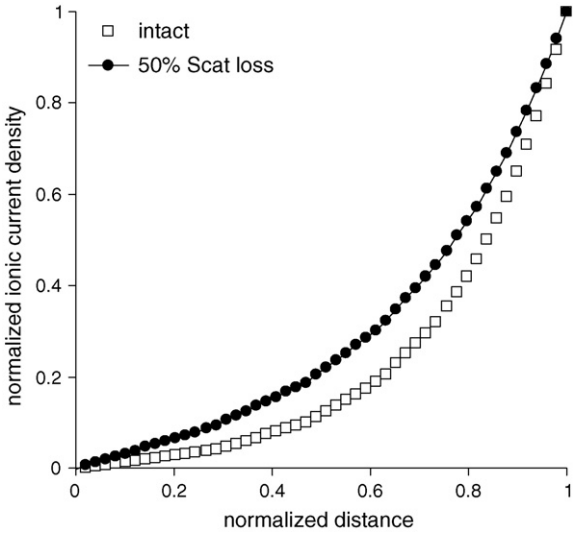

Fig. 13. Change in normalized ionic current density distribution over the cathode thickness for a thick (100 μm) cathode, resulting from the uniform loss of 50% of its surface area. This mechanism spreads the ionic current density over a larger extent away from the electrolyte.

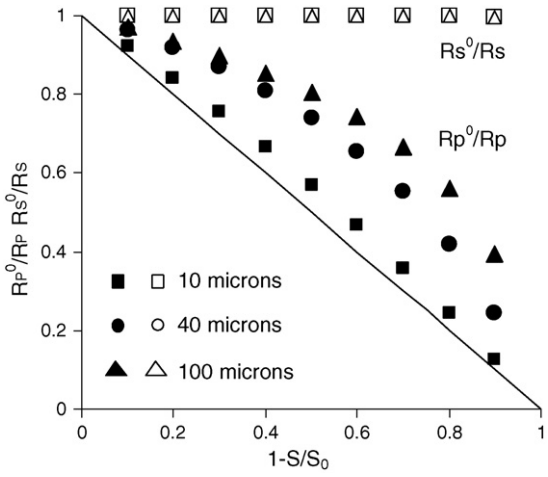

Fig. 14. Normalized polarization resistance (solid symbols) and normalized series resistance (open symbols) as a function of the fraction of uniform surface area loss in the cathode for different cathode thicknesses in an ESC. The line S/S_0 is plotted for comparison. The thinner the electrode, the more severe (i.e. closer to the S/S_0 line) the extent of degradation.

Thin electrodes are more completely utilized in the intact state, and therefore their performance degradation due to surface area loss is more abrupt. Fig. 14 illustrates this statement with a comparison of series and polarization resistance changes for cathodes of different thicknesses: 10, 40, and 100 μm. The solid symbols indicate the trend in polarization resistance. The deterioration is more abrupt for thin cathodes (squares) than for thick cathodes (triangles). The series resistance (open symbols) remains unchanged in all cases, as expected. A uniform surface area loss will therefore cause only a change in R_P of the affected electrode and not in R_S, and the extent of change in R_P may be significantly smaller than that of the loss in surface area, particularly for thick electrodes. Delaminated cells, on the other hand, will experience a simultaneous change in series and in polarization resistances of both electrode arcs, and the change in both R_S and R_P will be in the same proportion as that of the delaminated area fraction. This behaviour, therefore, is a distinct signature of delamination. Also, the change in impedance behaviour caused by delamination is not dependent on electrode thickness, as opposed to uniform surface area loss caused by poisoning or nickel sintering, which causes slightly less severe changes in polarization resistance for thick electrodes than for a delamination of the equivalent surface area. There is no corresponding change in the series resistance for the case of uniform surface area loss distributed through the electrode volume. Although a reduction in electroactive surface area could also imply a reduction in porosity (as would occur with nickel sintering in the anode), no observable change in series resistance was found between ASCs with 40% and with 20% anode porosity. Despite the change in effective conductivity that results from a decrease in porosity, the primary contributor to the R_S in a single cell is the electrolyte, even for an ASC.

3.3. Change in characteristic frequency

Delamination causes active area loss without altering the nature of the cell electrochemical processes. As a consequence,

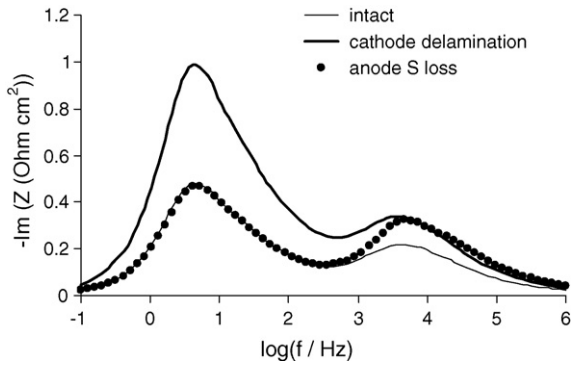

Fig. 15. Imaginary impedance as a function of logarithm of frequency, showing that the peak frequencies of the electrode processes remain unchanged for 50% cathode delamination, while the magnitudes of both electrode impedances change with delamination of either electrode (cathode delamination shown). The magnitude of electrode impedance caused by uniform surface area loss changes only for the corresponding electrode (70% anode surface area loss shown).

it is expected that the electrode characteristic frequencies remain unaffected by delamination. The model results support this hypothesis for a 50% loss in the electrode area by delamination, as illustrated in Fig. 15, bold lines. This figure shows the imaginary part of the impedance as a function of the frequency, in logarithmic scale, for a simulation performed at a DC voltage of 0.7 V. Although the imaginary impedance increases in magnitude with such a large delamination area, both electrode peak frequencies remain constant. Furthermore, both electrode peaks increase for a delamination of either electrode.

On the other hand, the equivalent graph for loss of 70% of the active surface area in the anode (dots in Fig. 15) shows a shift in peak frequency of the anode maximum. Furthermore, only the magnitude of the imaginary impedance corresponding to the anode process increases in the case of the uniform anode surface area loss, and it takes a larger amount of surface area loss to produce an increase in the anodic polarization resistance equivalent to that produced by delamination. Such a large extent in degradation is chosen to facilitate the visualization of the results. An underlying assumption for this calculation is that the double layer capacitance per unit area (F m^{-2}) remains unaltered. This assumption is equivalent physically to assuming that a fraction of the sites are completely covered and no longer participating in the electrochemical reaction in the case of a poisoning degradation mode, with the remaining sites remaining electrochemically unaltered, or to a coarsening of the anode microstructure with no corresponding change in the mechanism of the electrochemical reactions occurring on the remaining electrochemically active surface area.

Thus, an increase in polarization resistance of both electrodes with no corresponding changes in peak frequency, when accompanied by a proportional increase in series resistance, is a characteristic of a delaminated single solid oxide fuel cell that can be utilized to distinguish that mode of cell degradation from others causing a loss in surface area.

As far as the identification of surface area loss is concerned, it is possible, in principle, to identify uniform surface area loss occurring in an electrode as long as its characteristic arc is distinguishable from that of the other electrode. This requirement implies presenting a large enough difference in characteristic frequencies. If this is the case, an increase in diameter of only the arc(s) corresponding to one electrode in a Nyquist plot, or of magnitude of imaginary impedance of one electrode in a plot of imaginary impedance as a function of frequency, is evidence of degradation of this electrode by loss of surface area. Even in the case of distinguishable electrode arcs, the presented model is currently unable to distinguish between different uniform surface area loss mechanisms that could potentially affect one given electrode. For example, equivalent amounts of uniform surface area loss caused by anode sintering or anode sulphur poisoning would result in similar changes in the impedance spectrum under the conditions studied. Further development of the technique to include diffusion effects in the electrochemical model and to correlate surface area loss due to sintering with the corresponding porosity changes, could potentially provide a way to distinguish among these two anode degradation mechanisms. Further work is under way to extend the diagnostic technique to the prediction of stack-level degradation involving interconnect oxidation or loss of contact.

4. Conclusions

An impedance model of an operating SOFC has been developed that allows the identification of diverse degradation mechanisms in a non-invasive way. The method is based on the recognition of distinct changes in the impedance spectrum produced by each type of degradation mode.

Degradation mechanisms such as delamination and electrode sintering or poisoning result in the loss of reaction sites because of the loss in active area. Even when those mechanisms produce the same DC effect, namely a loss in potential at a given load, the resulting changes in the impedance spectrum are distinct. Delamination causes an almost complete loss of active area in the projected region above and below the delamination, due to the large aspect ratio of SOFCs that makes in-plane conduction of ionic species negligible, particularly for thin electrolytes. The implication on the change in impedance is that both series and polarization resistances change simultaneously and by approximately the same proportion. This result is observed for both anode and cathode delamination, the difference between which is likely too small to be detected experimentally. There is no change in the electrochemistry of the system upon delamination, and consequently the peak frequencies of the electrode arcs remain unchanged. Layer thicknesses do not influence the detectability of delamination using the present method unless the electrode thickness becomes very thin and therefore underutilized in its intact state, in which case the induced change is larger in magnitude, while maintaining the same proportion with respect to the intact electrode polarization resistance, and therefore is easier to detect. For thin electrolyte configurations, the series resistance change may potentially be too small to be detected reliably in a working cell.

Surface area loss, on the other hand, causes a less severe degradation for a given uniform active area loss distributed evenly through the electrode volume, when compared with delamination. This is especially the case in cells with thick

electrode geometries, in which a redistribution of the electrochemical activity over the electrode volume is observed. No change is induced in the series resistance in the case of uniform surface area loss in the electrodes, since the conduction path remains unaltered. If only one electrode suffers from this degradation, only its corresponding impedance arc increases in size, and its peak frequency changes as well, while in the case of delamination, both electrode arcs change if either electrode suffers delamination, while the peak frequencies remain unchanged. The degradation caused by a uniform loss in surface area is increasingly more serious for thin electrodes.

Therefore, using the results of the electrochemical impedance model presented here, a strategy for distinguishing between individual degradation modes corresponding to cathode or anode delamination or poisoning or sintering can be used to identify the causes of voltage degradation over time, and to identify strategies for reversing those degradation modes that can be alleviated through a change in operating conditions, while identifying permanent modes of degradation in an operating fuel cell that require disassembly of the stack and replacement of damaged cells.

References

[1] J. Koh, B. Kang, H. Lim, Y. Yoo, Electrochem. Solid-State Lett. 4 (2) (2001) A12–A15.
[2] S. Xia, V. Birss, Proc. SOFC IX 2 (2005) 1275–1283.
[3] E. Ivers-Tiffée, Q. Weber, D. Herbstritt, J. Eur. Ceram. Soc. 21 (2001) 1805–1811.
[4] J. Gazzarri, O. Kesler, Proc. 35th Conf. of Metallurgists, Calgary, AB, 2005.
[5] J. Bentzen, J. Bilde-Soerensen, Y. Liu, M. Mogensen, Proc. 26th Risoe International Symposium on Materials Science, Roskilde, Denmark, 2005, pp. 127–132.
[6] T. Iwata, J. Electrochem. Soc. 143 (5) (1996) 1521–1525.
[7] J. Newman, C. Tobias, J. Electrochem. Soc. 109 (12) (1962) 1183–1191.
[8] E. Barsoukov, J. MacDonald (Eds.), Impedance Spectroscopy, 2005, p. p. 87.
[9] S. Singhal, K. Kendall (Eds.), High-temperature Solid Oxide Fuel Cells: Fundamentals, Design and Applications, Elsevier, Oxford, 2003, p. 73.
[10] S. Primdahl, M. Mogensen, J. Appl. Electrochem. 30 (2000) 247–257.
[11] M. Juhl, S. Primdahl, C. Manon, M. Mogensen, J. Power Sources 61 (1996) 173–181.
[12] M. Jørgensen, S. Primdahl, M. Mogensen, Electrochim. Acta 44 (1999) 4195–4201.
[13] M. Jørgensen, M. Mogensen, J. Electrochem. Soc. 148 (5) (2001) A433–A442.
[14] J. Deseure, Y. Bultel, L. Dessemond, E. Siebert, Electroch. Acta 50 (2005) 2037–2046.
[15] T. Kawada, N. Sakai, H. Yokokawa, M. Dokiya, J. Electrochem. Soc. 137 (10) (1990) 3042–3047.
[16] B. Kenney, K. Karan, Proceedings of Hydrogen and Fuel Cells 2004, 2004, pp. 1–11.